General Disclaimer

One or more of the Following Statements may affect this Document

- This document has been reproduced from the best copy furnished by the organizational source. It is being released in the interest of making available as much information as possible.

- This document may contain data, which exceeds the sheet parameters. It was furnished in this condition by the organizational source and is the best copy available.

- This document may contain tone-on-tone or color graphs, charts and/or pictures, which have been reproduced in black and white.

- This document is paginated as submitted by the original source.

- Portions of this document are not fully legible due to the historical nature of some of the material. However, it is the best reproduction available from the original submission.

Final Report on Work Done on

CONTROL OF A FLEXIBLE ROBOT ARM

Under Contract #955636

By :   Eric Schmitz
         Robert Cannon

January 1980

Stanford University
Stanford, California

TABLE OF CONTENTS

I. INTRODUCTION

A. Importance of flexible arm control to robotics.

Today's manipulator systems are really quite crude. They tend to be massive and ponderous. In industrial applications, manipulators weighing tons are required to transport and position parts and tools weighing a few pounds. They are, therefore, costly in the materials used to make them, the space they take up, the power they consume, and the time they require to do simple operations.

The Space Shuttle manipulator will have to be operated manually and very slowly.

To date, the growing computer power available has been used to handle kinematic relations of increasing complexity. But problems of dynamics and flexibility have been solved by making the members extremely stiff. As we become able to develop control techniques that tolerate flexibility in a manipulator's mechanical structure, the use of such flexible arms will have many desirable consequences: manipulators can be lighter and faster, safer to use, and less prone to damage from collisions. They will also require less power to run and cost less to construct. They will be essential to the objective of automating the tasks of the large, flexible manipulator arms of the Space Shuttle. Finally, these same control strategies will be important for the control of such flexible space structures as very large antennas: large space systems planned for the 1980's and beyond will require significant advances over today's technology.

Another characteristic of today's manipulators is that they effect position control by "dead reckoning": the computer is told the coordinates of the desired position, and the manipulator

system is moved by controlling the angle of each link relative to the previous one. Position accuracy is thus only as good as the accumulation of errors and the stiffness of the members, and of the base on which everything sits. The astute use of end-point sensins and feedback will make possible a new level of precision in manipulator use, and open up many new areas for manipulator application. For space applications -- where the "base" is empty space, the manipulator links are highly flexible, and the penalty for inaccuracy may be either painfully slow operation or destruction of delicate space systems -- sophisticated end-point feedback will be an essential element.

A third very important problem that limits the capability of present manipulators is the fact that there are large, and rapid changes can occur in the inertia properties of the system being controlled as it changes configuration, and particularly when it picks up massive loads. Precise control of a system having large time variation in its parameters is a particularly nasty problem. If constant control "gains" are used the system response will necessarily vary from very sluggish to nearly unstable. If a scheme of total adaption is used, an essential nonlinearity is introduced which makes the control algorithm extremely complex. Our recent work in the areas of optimal control with uncertain parameters and plant identification leads us to believe the best control strategy for the manipulator control problem will be a combination of adaptation by regime and robust optimal control within regimes. (This also will introduce some challenging switching problems; but the tradeoff appears favorable.)

B. Long-term goals.

What we propose to do together in the present project is to bring to bear (1) experience with dynamics and control of flexible structural members, (2) end-point sensing techniques, and (3) advanced concepts for robust control of systems whose parameters are uncertain and changing, to demonstrate good control of a single, very flexible member in a plane. Then a mass of unknown size (object to be carried) will be added at the end of the arm, so that the controller must infer the new dynamic character of the system quickly enough to accomplish fast, efficient transport to a commanded location, and precise final positioning.

C. Initial objectives for this contract.

a. Develop and analyze exact equations of motion of an arm with known parameters preparatory to designing control systems for same.

b. Design an experimental one-link arm for testing control designs.

II. ANALYSIS OF A CONTROLLABLE FLEXIBLE ROBOT ARM.

A. Modal equations.

The goal is to describe the motion of the arm by a set of first order differential equations in the following manner:

(I)
$$\dot{x} = Fx + Gu$$
$$y_s = Hx$$

x is the state vector $x^T = q_0, \dot{q}_0, q_1, \dot{q}_1, q_2, \dot{q}_2, \ldots$ where q_0 describes the rigid body mode

q_i, $i \geq 1$ describes the i-th flexible mode

u is the control torque

y_s is a vector made up of the 3 outputs of the 3 sensors mounted on the beam

The rationale for such a formulation (I) is that it is the most convenient form for using modern control design techniques.

i. Development of the equations of motion.

The model for the arm is a uniform beam of length ℓ, density ρ, width b and thickness t and elasticity modulus E with a lumped inertia at its hub I_H.
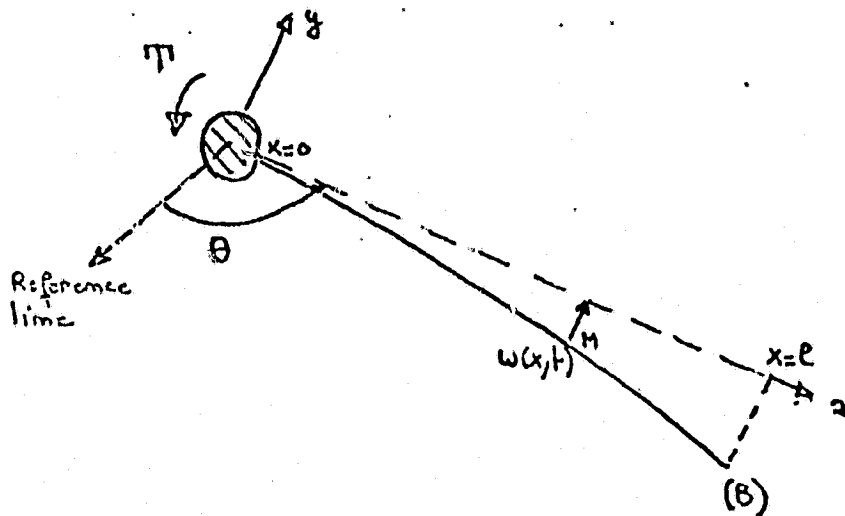

FIG. 1. Geometric Definitions

The equations are obtained from the angular momentum theorem and Hamilton's principle.

From angular momentum theorem:

(1) $\quad \dfrac{dh}{dt} = T \qquad$ where $h = \left| \displaystyle\int_{(a)} (\overrightarrow{om} \times \vec{v})\,dm \right| + I_H \dot{\theta}$

we have $v = -\omega\dot{\theta}\vec{x} + (\dot{\omega} + x\dot{\theta})\vec{y}$

so $\quad h = \displaystyle\int_0^\ell (x\dot{\omega} + x^2\dot{\theta})\,dm + I_M\dot{\theta} \quad$ after neglecting $\omega^2\dot{\theta}$

From (1) we get:

(2) $\qquad \displaystyle\int_0^\ell x\ddot{v}\,dm + \left(I_B + I_H\right)\ddot{\theta} = T$

From Hamilton's principle:

(3) $\qquad \delta\left(\displaystyle\int_{t_1}^{t_2} L\,dt \right) = 0 \quad$ where L is the lagrangian of the arm; $\delta\theta$ and δw are virtual displacements which are 0 at t_1 adn t_2. If we call y : $y = w + x\theta$ y can be large as the angle θ becomes large; w remains small.

The Lagrangian $L = T_k - V$ is made up of 2 terms:

- kinetic erergy -

(4) $\qquad 2T_k = I_H\dot{\theta}^2 + \displaystyle\int_0^\ell \left(\dfrac{\partial y}{\partial t}\right)^2 dm \qquad$ after neglecting

the centrifugical term $\omega^2\dot{\theta}$

- potential energy V -

(5) $\qquad 2V = \displaystyle\int_0^\ell E_I\left(\dfrac{\partial^2 y}{\partial x^2}\right)^2 dx - T\theta$

This expression is valid if $\dfrac{\partial w}{\partial x}$ and $\dfrac{\partial^2 w}{\partial x^2}$ remain small (Euler-Bernouilli beam)

After many manipulations on (3) with (4) and (5) we get a 4th order PDE describing the beam.

(6)
$$EI \frac{\partial^4 y}{\partial x^4} + \rho \frac{\partial^2 y}{\partial t^2} = 0$$

$$EI \frac{\partial^2 y}{\partial t^2}\bigg|_0 + T = I_H \ddot{\theta}$$

$$y(0) = 0$$

$$\frac{\partial^2 y}{\partial x^2}\bigg|_{x=\ell} = \frac{\partial^3 y}{\partial x^3}\bigg|_{x=\ell} = 0$$

Note that the 1st equation could be written in terms of the

small quantity w:
$$EI \frac{\partial^4 y}{\partial x^4} + \rho \frac{\partial^2 w}{\partial t^2} = -\rho x \ddot{\theta}$$

(2) and (6) describe completely the dynamics of a uniform one

link arm.

ii. Natural modes of the arm:

In order to get the natural frequencies and mode shapes of the arm we set the control torque T to zero in (6) and write $y(x,t) = \phi(x)q(t)$ where $q(t) = e^{i\Omega t}$

(6) can be written as:

$$\frac{d^4\phi}{dx^4} - \beta^4\phi = 0$$

$$EI\,\phi''(0) = -I_H\,\Omega^2\phi'(0) \quad (7) \qquad \beta^4 = \frac{\rho\Omega^2}{EI}$$

$$\phi(0) = 0$$

$$\phi''(\ell) = \phi'''(\ell) = 0$$

The solution to (7) is:

$$\phi(x) = A\cos\beta x + B\sin\beta x + C\cosh\beta x + D\sinh\beta x \qquad (8)$$

The frequencies Ω_i are solution of the equation:

$$\cos\lambda_i\sinh\lambda_i - \sin\lambda_i\cosh\lambda_i - \epsilon\lambda_i^3(1 + \cos\lambda_i\cosh\lambda_i) = 0 \qquad (9)$$

where $\lambda_i^4 = \frac{\rho\ell^4}{EI}\Omega_i^2$ and $\epsilon = I_H/3I_B$
I_H = hub inertia
I_B = beam inertia

In order to get the 4 constants A,B,C,D we need to normalize the mode shapes:

$$\int_0^\ell \phi_i^2(x)\,dx + \frac{I_H}{\rho}\left[\phi'(0)\right]^2 = \frac{I_H + I_B}{\rho} \,^{(*)}, \quad i = 0,1,\dots\infty \qquad (10)$$

A numerical program has been written to solve for (9) and (10). Table 1 contains four different values of ϵ, the values of λ_i $\left(\lambda_i^4 = \frac{\rho\ell^4}{EI}\Omega_i^2\right)$ and A,B,C,D for the first 4 mode shapes.

* for the rigid body mode: $\phi_0(x) = x$

ε	Mode #	λ	A	B	C	D	δᵢ
0	1	3.327	0.	0.	1.414	-0.039	1.8
"	2	7.068	0.	0.	1.414	-0.017	3.336
"	3	10.214	0.	0.	1.414	-0.001	4.813
"	4	13.352	0.	0.	1.414	0.	6.294
0.02	1	3.4	0.465	-.465	1.163	0.431	1.635
"	2	5.201	-1.197	1.197	0.217	-1.204	-1.629
"	3	7.364	-1.091	1.091	0.870	-1.091	-.582
"	4	11.034	-1.025	1.035	0.358	-1.035	-.284
0.04	1	3.078	0.760	-0.760	0.606	0.696	1.336
"	2	4.35	-1.123	1.123	0.673	-1.136	-0.764
"	3	7.302	-1.041	1.041	0.335	-1.04	-0.277
"	4	11.014	-1.016	1.016	0.378	-1.02	-0.140
0.06	1	2.878	0.836	-0.836	0.407	0.752	1.121
"	2	4.842	-1.093	1.093	0.721	-1.107	-.514
"	3	7.282	-1.027	1.027	0.957	-1.027	-.183
"	4	11.008	-1.011	1.011	0.386	-1.011	-.093
0.08	1	2.74	0.876	-0.876	0.272	0.752	0.872
"	2	4.813	-1.073	1.073	0.849	-1.029	-0.385
"	3	7.881	-1.021	1.021	0.968	-1.02	-0.137
"	4	11.005	-1.01	1.01	0.989	-1.01	-0.069
0.1	1	2.633	0.900	-0.900	0.171	0.808	0.862
"	2	4.794	-1.060	1.060	0.24	-1.077	-.308
"	3	7.876	-1.02	1.02	0.974	-1.016	-.109
"	4	11.003	-1.01	1.01	0.991	-1.01	-.055

Table 1   Mode shapes coefficients
(δᵢ is defined later in equation 12)

Revision: A, B, C, D should be multiplied by $\frac{\sqrt{1+3\epsilon}}{\sqrt{3}}$

δᵢ should be multiplied by $\sqrt{2(1+3\epsilon)}$

FIRST TWO MODE SHAPES

MODE SHAPE #1

MODE SHAPE #2
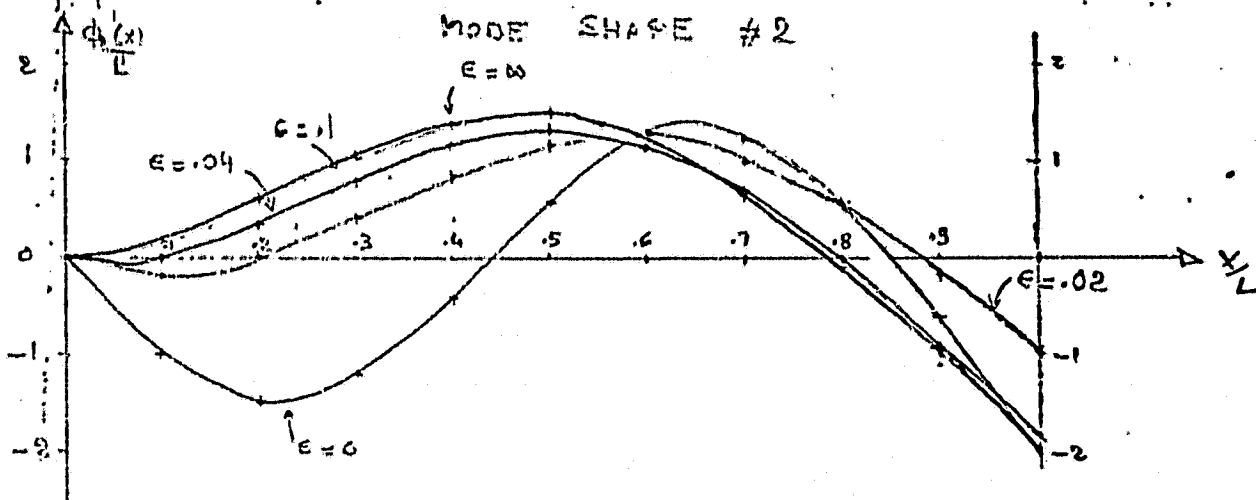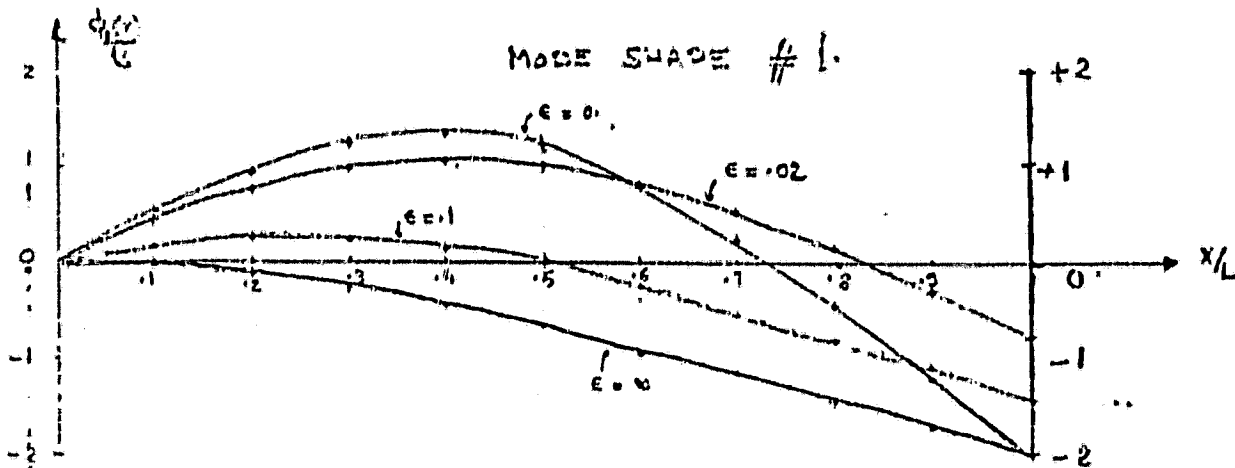
Note: $\epsilon = \dfrac{I_{Hub}}{3\, I_{Beam}}$

$\epsilon = 0$ ⟶ pinned-free beam

$\epsilon = \infty$ ⟶ cantilevered beam
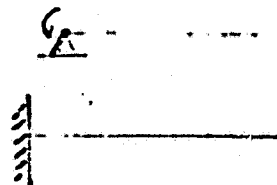
iii. Modal equations.

We now proceed to get the set of ODE's we are looking for.

We write the solution $y(x,t)$ to (6) as:

$$y(x,t) = \sum_{i=0}^{\infty} \phi_i(x)\, q_i(t)$$
$$= x q_0 + \sum_{i=1}^{\infty} \phi_i(x)\, q_i(t)$$

We re-write (3) and (4) (including control torque) as: $2L = 2T_k - 2V$

$$2L = \sum_{ij} \left[I_H \phi_i^x(0)\, \phi_j^x(0)\, \dot{q}_i \dot{q}_j \right] + \sum_{ij} \left[\int_0^\ell \phi_i \phi_j\, dm\; \dot{q}_i \dot{q}_j \right]$$
$$- EI \sum_{ij} \left[\int_0^\ell \phi_i^{xx} \phi_j^{xx}\, dx\; q_i q_j \right] + T\theta$$

Using the orthogonality relations, we obtain the relations:

$$\int_0^\ell \phi_i \phi_j\, dm + I_H \phi_i^x(0)\, \phi_j^x(0) = (I_H + I_B)\, \delta_{ij} \qquad i,j \neq 0$$

$$\int_0^\ell \phi_0^2\, dm + I_H \left[\phi_0^x(0) \right]^2 = I_H + I_B$$

$$EI \int_0^\ell \phi_i^{xx^2} \phi_j^{xx^2}\, dx = (I_H + I_B)\, \Omega_i^2\, \delta_{ij} \qquad i,j \neq 0$$

so, we get:

$$2L = (I_H + I_B)\, \dot{q}_0^2 + \sum_{i=1}^{\infty} (I_H + I_B)\, \dot{q}_i^2 - \sum_{i=1}^{\infty} (I_H + I_B)\, \Omega_i^2\, q_i^2 + T\left[q_0 + \sum_{i=1}^{\infty} \phi_i^x(0)\, q_i \right]$$

Lagrange's equations are:

$$\frac{d}{dt}\left(\frac{\partial L}{\partial \dot{q}_i} \right) - \frac{\partial L}{\partial q_i} = 0 \qquad i = 0, 1, \dots \infty$$

so:

$$(I_H + I_B)\, \ddot{q}_0 = T$$

$$\ddot{q}_i + \Omega_i^2\, q_i = \phi_i^x(0)\, \frac{T}{I_H + I_B} \qquad (11)$$

$$1 \leq i \leq \infty$$

Note: (11) is the same type of equation as the one used by Likins (see JPL Report on flexible s/c dynamics.)

It is possible to include damping:

$$\ddot{q}_i + 2\zeta \Omega_i\, \dot{q}_i + \Omega_i^2\, q_i = \phi_i^x(0)\, \frac{T}{I_H + I_B}$$

We write:

$$\ddot{q}_i + \Omega_i^2 q_i = \delta_i \frac{T}{I_H + I_B} \qquad \text{where} \quad \delta_i = \phi_i^z(0) \qquad (12)$$

$$y(x,t) = \sum_{i=0}^{\infty} \phi_i(x) q_i(t) = x q_0 + \sum_{i=1}^{\infty} \phi_i(x) q_i(t)$$

the δ_i's have been computed for different values of ϵ and are shown in Table 1.

iv. Measurement vector y_s:

The sensors that will be used to control the arm are a potentiometer (θ), a tachometer ($\dot{\theta}$), a tip sensor for terminal control at the end of the slew maneuver ($y(L)$) and a set of strain gages at different locations x_1.

From (12) we get:
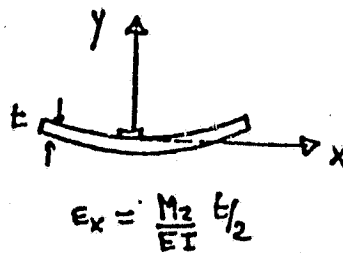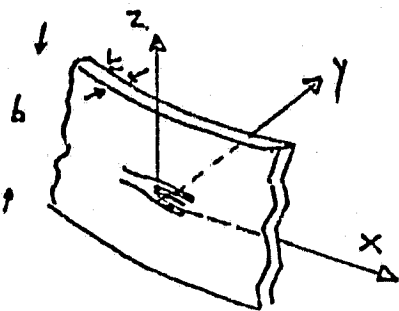
$$\theta = q_0 + \sum_{i=1}^{\infty} \delta_i q_i$$
$$\dot{\theta} = \dot{q}_0 + \sum_{i=1}^{\infty} \delta_i \dot{q}_i \qquad \text{where } \delta_L \text{ are shown in Table 1} \quad (14)$$

$$y_T = L q_0 + \sum_{i=1}^{\infty} \phi_i(L) q_i \qquad \text{where } \phi_1(L) \text{ are shown in Table 1.} \quad (1$$

The strain gages measure the strain at the surface of the beam:

$$\epsilon_x = \frac{M_z}{EI} \frac{t}{2}$$

The bending moment is: $M_z = EI \left. \dfrac{\partial^2 y}{\partial x^2} \right|_{x = x_1}$

so that: $\left. \sigma_x \right|_{x=x_1} = \dfrac{t}{2} \sum_{i=1}^{\infty} \left. \phi_i^{\prime\prime} \right|_{x=x_1} q_i$

B. Exact Transfer Functions for a One Link Arm.

From the dynamics equations developed in A, it is possible to obtain any transfer function from the control torque to any sensor output y_s^k; but, in order to do that, one has to truncate and keep a finite number of modes. This implies that the zero of the truncated T.F. will not be exact.

Alternatively, a technique shown by A. Bryson enables one to get exact T.F. for certain simple analytical models (i.e., Euler-Bernouilli Beams).

i. Transfer function calculation.

Let's take the Laplace's transform of the set of equations (6) in A and also change x to $x_1 = L - x$:

$$\frac{d^4y}{dx_1^4}(x_1,s) + \frac{\rho s^2}{EI} y(\ddot{x}_1, s) = 0$$

$$y^{II}(0,s) = y^{III}(0,s) = 0 \qquad \qquad (1)$$

$$T + EIy^{II} \cdot L,s = -I_H s^2 y^I(L,s)$$

$$y(L,s) = 0$$

Let's define $\beta \qquad \beta^4 = -\frac{\rho s^2}{EI}$ $\qquad \beta$ is a complex number

The first equation of (1) is: $y^{IV}(x^1,s) - \beta^4 y(x^1,s) = 0$

$$y(x^1,s) = A \sin(\beta x^1) + \beta \sinh(\beta x^1) + C \cos(\beta x^1) + D \cosh(\beta x^1)$$

Using the 4 boundary conditions in (1) we get: A = B; C = D

and the following 2 x 2 linear system:

$$\begin{bmatrix} \sin\lambda + \sinh\lambda & \cos\lambda + \cosh\lambda \\ -\sin\lambda + \sinh\lambda - \varepsilon\lambda^3(\cos\lambda+\cosh\lambda) & -\cos\lambda + \cosh\lambda - \varepsilon\lambda^3(\sin\lambda+\sinh\lambda) \end{bmatrix}\begin{bmatrix} A \\ C \end{bmatrix} = \begin{bmatrix} \\ E \end{bmatrix}$$

where: $\lambda = \beta L$ $\qquad \varepsilon = \frac{I_H}{\rho L^2} = \frac{I_H}{3 I_B}$ $\qquad$ (as in A)

We solve for this system and get the T.F. $y(x_1,s)/T$:

$$\frac{y(x',s)}{T} = \frac{(c\lambda + ch\lambda)(s\beta x' + sh\beta x') - (s\lambda + sh\lambda)(c\beta x' + ch\beta x')}{2 E I \beta^2 [s\lambda ch\lambda - sh\lambda c\lambda + \epsilon\lambda^3 (1 + c\lambda ch\lambda)]} \quad (2)$$

where: $c = \cos$; $s = \sin$; $ch = \cosh$; $sh = \sinh$

ii. Application.

We can get any T.F. of interest for any sensors.

a) Transfer function θ_H/T (potentiometer/tachometer at hub)

Note that $x^1 = 0$ at hub from $x^1 = L - x$

$$\theta_H = - \frac{\partial y}{\partial x^1}(L,s)$$

From (2) we get:

$$\frac{\theta_H}{T} = - \frac{1}{E I \beta} \frac{1 + c\lambda ch\lambda}{s\lambda ch\lambda - sh\lambda c\lambda + \epsilon\lambda^3(1 + c\lambda ch\lambda)}$$

λ is a complex number here: $\lambda^4 = - \frac{\rho L^4}{EI} s^2$; $s = j\Omega$
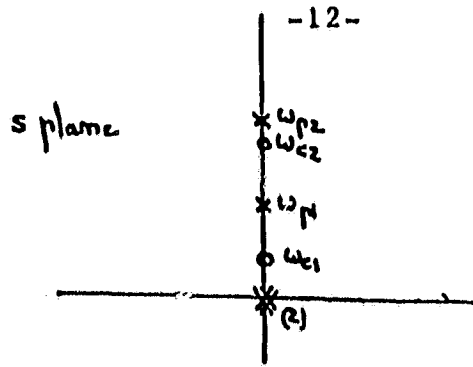
the numerator or the denominator

can be expanded as:

$$1 + c\lambda ch\lambda = 2 \prod_{i=1}^{\infty} \left(1 + s^2/\omega_{ci}^2\right)$$

$$s\lambda ch\lambda - sh\lambda c\lambda + \epsilon\lambda^3(1 + c\lambda ch\lambda) = \frac{2}{3} \lambda^3 \left[1 + \frac{I_H}{I_0}\right] \prod_{i=1}^{\infty} \left(1 + s^2/\omega_{pi}^2\right)$$

Finally, we get:

$$\frac{\theta_H}{T} = \frac{1}{(I_H + I_0)s^2} \frac{\left(1 + s^2/\omega_{c1}^2\right)\left(1 + s^2/\omega_{c2}^2\right) \cdots}{\left(1 + s^2/\omega_{p1}^2\right)\left(1 + s^2/\omega_{p2}^2\right) \cdots}$$

This transfer function is of very general application for any flexible body with co-located sensor (θ_H) and actuator (T).

s plane

If one excites the arm at the frequency of one of the zeros (w_{ci}) there will be no motion of the hub; of course, we have to include damping for real cases, so there will be small motion. This fact has been checked experimentally.

Note also that the zeros correspond to a cantilivered beam $(1 + c\lambda ch\lambda = 0$ is the well known equation for the frequencies of a cantilivered beam); the poles are for a pinned beam (if one set $\epsilon = 0$, $s\lambda ch\lambda - sh\lambda c\lambda$ is also well known to be for the pinned beam).

FIG. 1. shows the poles/zeros location for the model of the experimental beam.

It can be seen that for $\epsilon \geq 0.02$ from the third mode, poles and zeros cancelled each other.

B. Transfer Function y_T/T (tip sensor)

From (2): $y_T = y_T(x_1 = 0)$

so $y_T/T(s) = -\dfrac{1}{EI\beta^2} \dfrac{s\lambda + sh\lambda}{s\lambda ch\lambda - sh\lambda c\lambda + \epsilon\lambda^3(1+c\lambda ch\lambda)}$

, numerator and denominator can be expanded so that one gets the expression:

$$\frac{y_T}{T}(s) = -\frac{1}{(I_H+I_B)s^2} \frac{\left(1-\frac{s^2}{\omega_{z}^2}\right)\left(1-\frac{s^2}{\omega_{z2}^2}\right)\cdots}{\left(1+\frac{s^2}{\omega_{p1}^2}\right)\left(1+\frac{s^2}{\omega_{p2}^2}\right)\cdots}$$
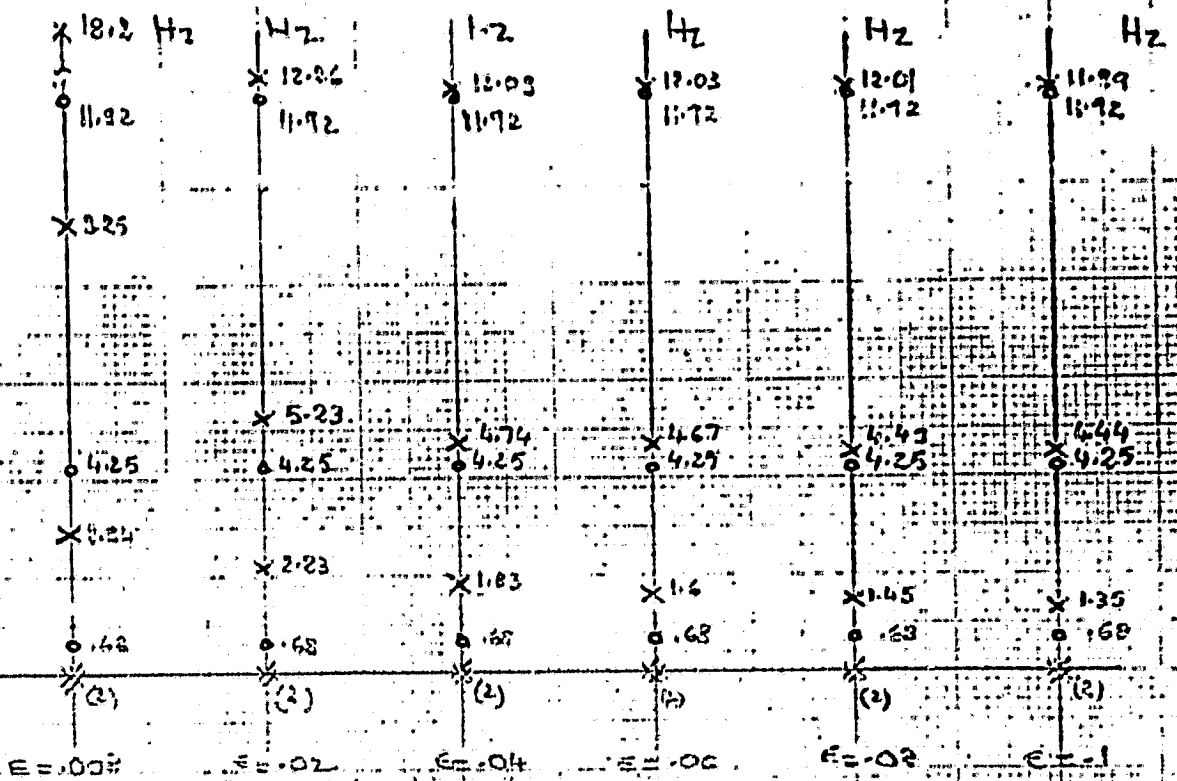
FIG 1   Poles / zeroes configuration for $\theta_H/_\pi$ $\left[\epsilon = \dfrac{I_{Hub}}{3 I_{Beam}} \right]$
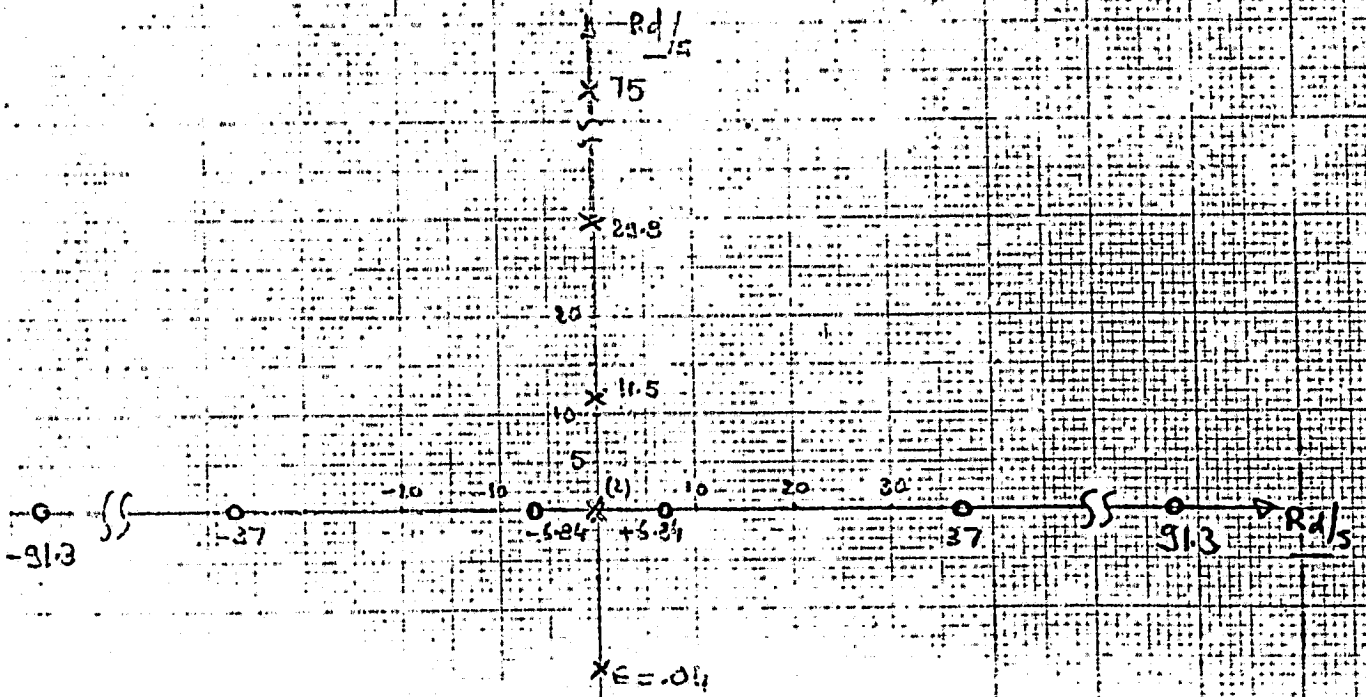

FIG 2   Poles / zeroes configuration for $y_\pi/_\pi$ (tip sensor)

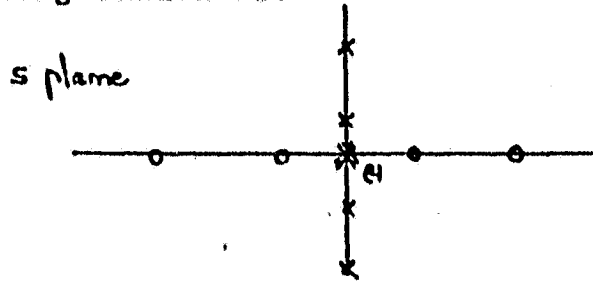Note: Zero locations don't depend on ϵ.

The configuration is:

FIG. 2. shows the configuration for the model of the exper-imental arm. It has been checked experimentally that there are no zeros on the jω axis; it seems difficult to verify _in open loop_ the (real axis) location of the zeros.

The zeros have been computed numerically:

$$\lambda_i = 2.365, \ 5.498, \ 5.498 + k\pi, \quad k>2$$

Then we get: $\omega_i^2 = \dfrac{EI}{\rho L^4} \lambda_i^4$

Conclusion.

We get a tool to design controllers for the arm using the root locus method and without having to bother with truncation errors. Note that it has been possible only because we have a very simple model: it cannot be applied to complicated structures.

III.   DESIGN OF EXPERIMENTAL APPARATUS.

Subsequent to the contract work reported here, a one link robot arm has been designed and built (under separate funding) by Moshe Tkacz, PhD candidate in the Department of Aeronautics & Astronautics.   The main problem to solve for the design of a very flexible arm is to make it rigid in torsion; if one uses a simple beam of 1 meter long, when the beam bends, the tip part of the beam deflects in torsion.   For decoupling of bending and torsion, the arm is made of 2 parallel beams connected together with 5 bridges; these bridges act as pinned joints for the bending of the 2 beams, and prevent any torsion of the arm. Picture 1 explains the arrangement:
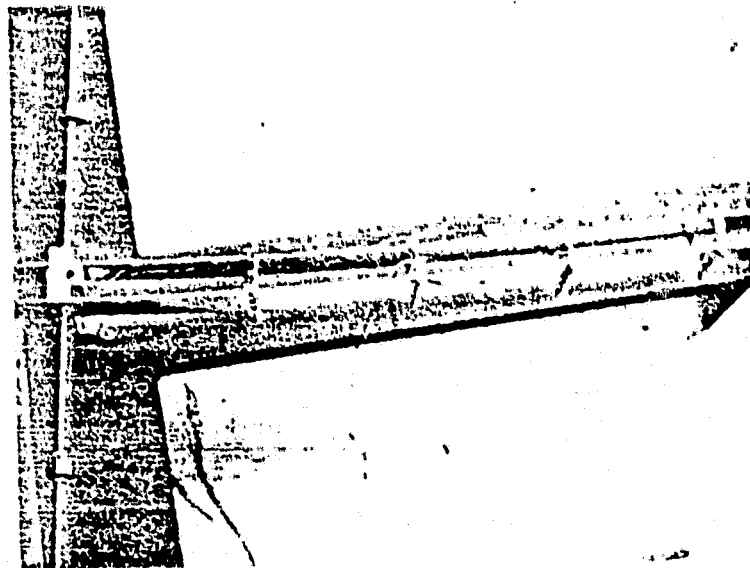
Picture 1:   Experimental arm (top view)

A. Arm Characteristics.
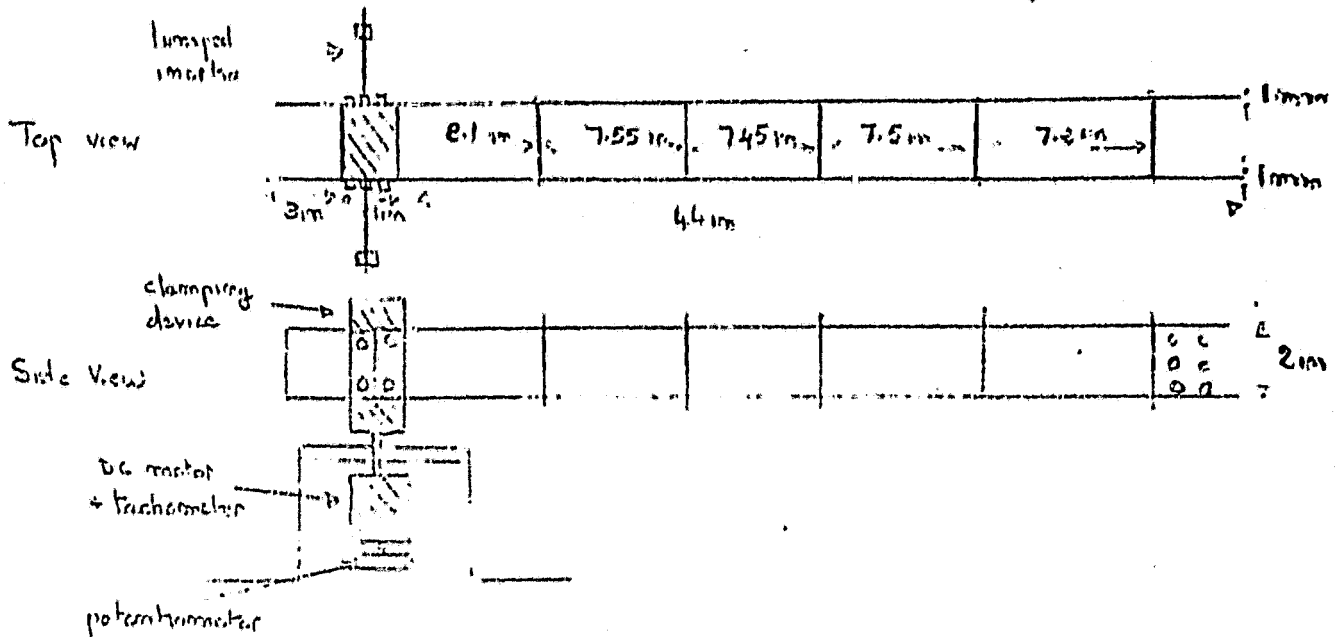
Below is the main data for the arm:

Beams mass: 2 x 6.5oz. = 373.6 g.   (I2gr)
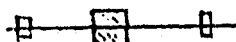
Bridges mass: 5 x 10 oz. = 141.5 g.   (made of berylium + Alu)

Bridge mass/Beam mass = .38

Beams moment of inertia at hub = .142 Kgm^2

Bridges moment of inertia at hub = .052 Kgm^2

Total arm moment of inertia I_B = .194 Kgm^2

Clamping device moment of inertia (hub) = 3.4 10^{-4} Kgm^2

Added inertia at the hub: ⊟–▦–⊟   .02 Kgm^2

Total hub inertia (including DC motor rotor & tachorotor) = .02I Kg

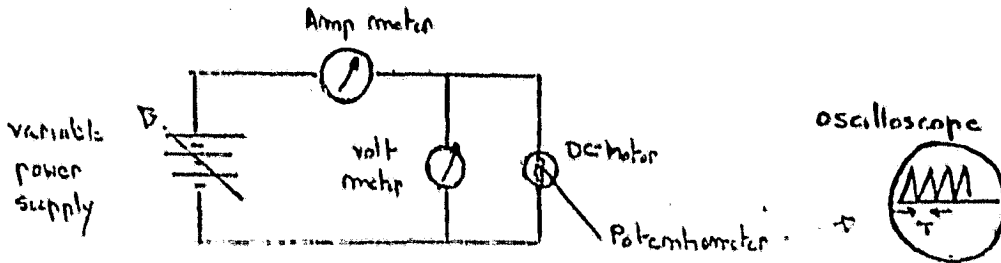Ratio ε (see II): $\varepsilon = \dfrac{I_H}{3I_B} = .036 \rightarrow .04$

Elasticity modulus: E = 7 10^{10} SI

Area moment of inertia: $I_{zz} = \dfrac{t^3 b}{12} = 4.33 \ 10^{-12} m^4$

EI = .296 Nm^2

B. Actuator Characteristics.

It's a MAGTECH 300 ozin peak torque DC servomotor. The main test performed on the motor is described in the next figure.

From this test, it was found that the back emf constant K_B is $K_B = .26$ Nm/A. It is the nominal value from the spec sheets. The theory says that the torque constant K_T and the constant K_B are equal: K_T(Nm/A) $= K_B$(V/Rd/s) so $K_T = .26$ Nm/A or $K_T = 37.2$ ozin/A.

A direct measurement of K_T should be performed in the future. Note that K_T is essential for a control design (gains). Also, a model of the actuator might be needed in the future $(\frac{K}{1+Ts})$.

C. Power Amplifier.

The PA enables one to have a current-drive DC motor, so that one can write: Torque $= K_T$ x Amperage.

The gain of the PA has been measured: $K_{PA} = 0.81$ A/V.

The dynamic model for the PA will be obtained.

D. Tachometer.

The tachometer is a DC motor (MAGFLEX).

The gain has been measured $K_{Tacho} = .06$V/Rd/s.

E. Potentiometer.

This is a Bourns single-turn film 20K potentiometer. The gain is K_{POT} = 4.77 V/Rd. A new potentiometer is on order because of the very noisy signal of the current one.

F. End Point Sensor.

This is a United Technology dual axis position sensor which provides x and y axis position of a light spot on the detector surface. One AC line-powered amplifier is used for each channel. The amplifiers provide 2 output voltages corresponding to the sum (light-intensity) and to the difference (position) of the 2 input currents.

A divider network is added to obtain a voltage directly proportioned to the position.

The light bulb has been mounted on the tip of one of the 2 beams. A lens of 22mm focal length focuses the image of the light bulb on the detector itself.

The gain of the tip sensor is:

K_{Ts} = .7 V/in   with divider   noise level .1V

K_{Ts} = .06 V/in   without divider   noise level .008V

Note that the sensor picks up all the ambient light and one needs to work in a dark environment for better results.

G. Strain Gages.

Two strain gages have been mounted at 19 in. from the hub on two sides of one beam; with two strain gages, one gets rid of the temperature effects.

The spec. for the gage itself is: $R = 120^{\Omega}t \cdot 5\%$

gage factor $K = 2.1t \cdot 5\%$

A CALEX bridge sensor is used as an amplifier and also to provide a regulated power supply for the wheastone bridge used for signal detection.

Currently, the setup is working with one strain gage put in the wheastone bridge. Calibration tests will be done and also frequency response tests will be done in open loop to check the validity of the analytical model.

Conclusion.

Many sensors are now available for control purposes. This implies that we will be able to be relatively immune to errors between the model and the actual plant.

We will also add variable low pass filters to get rid of the high frequency noise generated by all these sensors.

IV. A REPORT ON WORK DONE SUBSEQUENT TO THIS CONTRACT.

The apparatus described in Section III was subsequently built under separate funding.

The arm's natural frequencies have been measured for comparison with the analysis of Section II: this has been done by recording the gain curve of the transfer function θ_H/T, where θ_H is the output of the potentiometer. The analytical model yields an expression:

$$\frac{\theta_H}{T} = \frac{1}{(I_H + I_B) s^2} \frac{(s^2/\omega_1^2 + 1)(s^2/\omega_2^2 + 1) \cdots}{(s^2/\Omega_1^2 + 1)(s^2/\Omega_2^2 + 1) \cdots}$$

A constant amplified sinusoidal signal has been input to the entry point of the power amplifier. The output of the potentiometer was recorded on the oscilloscope. The frequency of the input signal was varied from .2 to 10 Hz. The zeros of the T.F. are the ones for which the output of the potentiometer is a local minimum while the poles are the ones for which it is a local maximum. Table 1 gives the comparison between experimental and theoretical values. The first theoretical zero ω_1 was assigned the experimental value (first bending frequency of the arm clamped).

zeros	theoretical	experimental	
	.68	.68	
	4.25	3.7	values are in Hz
poles	theoretical	experimental	
	1.83	1.9	
	4.74	4.2	

Table 1

RATE LOOP

3 flexible modes included (2 dispkaid)

FIGURE NO. 2

MIN GAIN,MAX GAIN,STEP SIZE
=5,6,0.5

GAIN	SYMBOL
1.000	
2.000	
3.000	
4.000	
5.000	
6.000	
7.000	
8.000	
9.000	
10.000	
5.000	
5.500	
6.000	

REAL
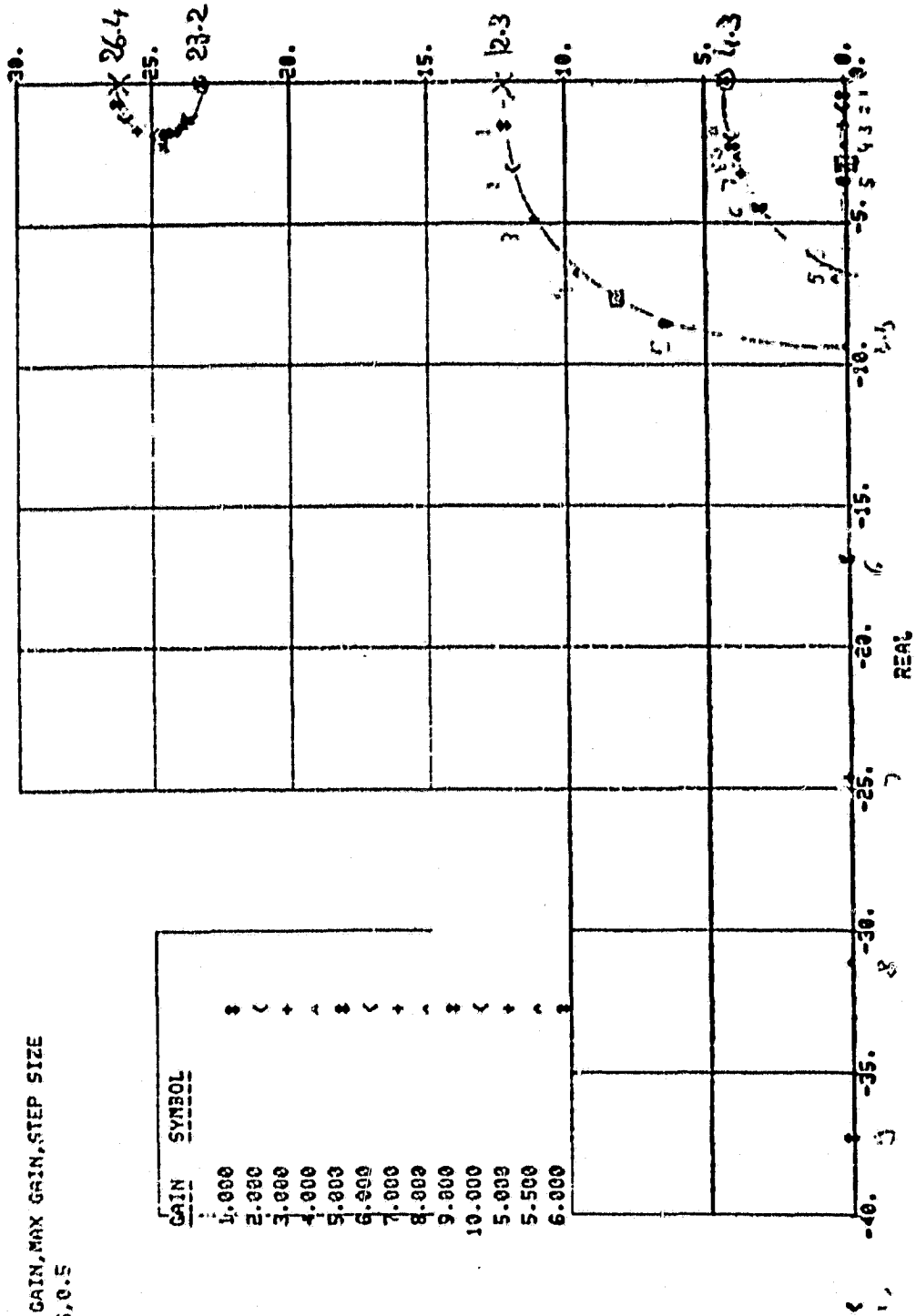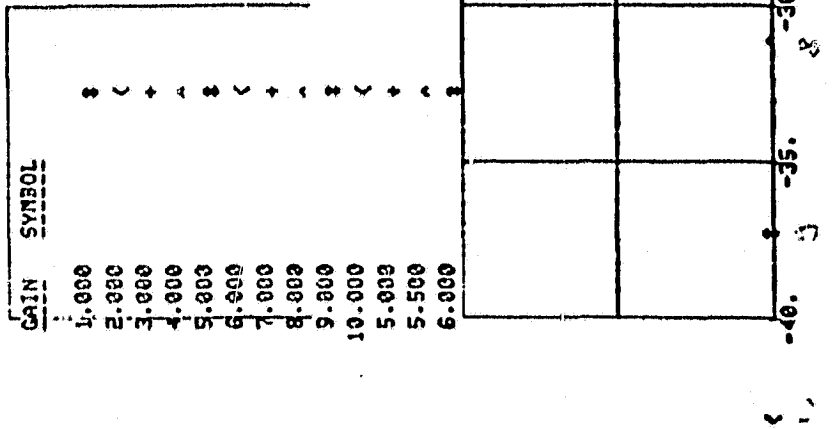
☒ closed loop poles location

Fig.2 Open loop zeroes

with lead $\dfrac{s+3}{s+30}$

FIGURE NO. 1

MIN GAIN,MAX GAIN,STEP SIZE

GAIN	SYMBOL
10.000	
20.000	
30.000	
40.000	
50.000	
60.000	
70.000	
80.000	
90.000	
100.000	

IMAGINARY

REAL

15.0   12.5   10.0   7.5   5.0   2.5

FIG 3   Tip sensor loop closure

The transfer ...
with lead $\dfrac{S+5}{S+30}$ - [imaginary ...]

FIGURE NO. 3

MIN GAIN,MAX GAIN,STEP SIZE

GAIN	SYMBOL
10.000	
20.000	
30.000	
40.000	
50.000	
60.000	
70.000	
80.000	
90.000	
100.000	

IMAGINARY

REAL

15.0

12.5

10.0

5.0

2.5

0.

-2.5

-5.0

-10.0   -7.5   -5.0   -2.5   0.   2.5   5.0   7.5   10.0

-6.3   -5   -2.73   6.8

Figure 4
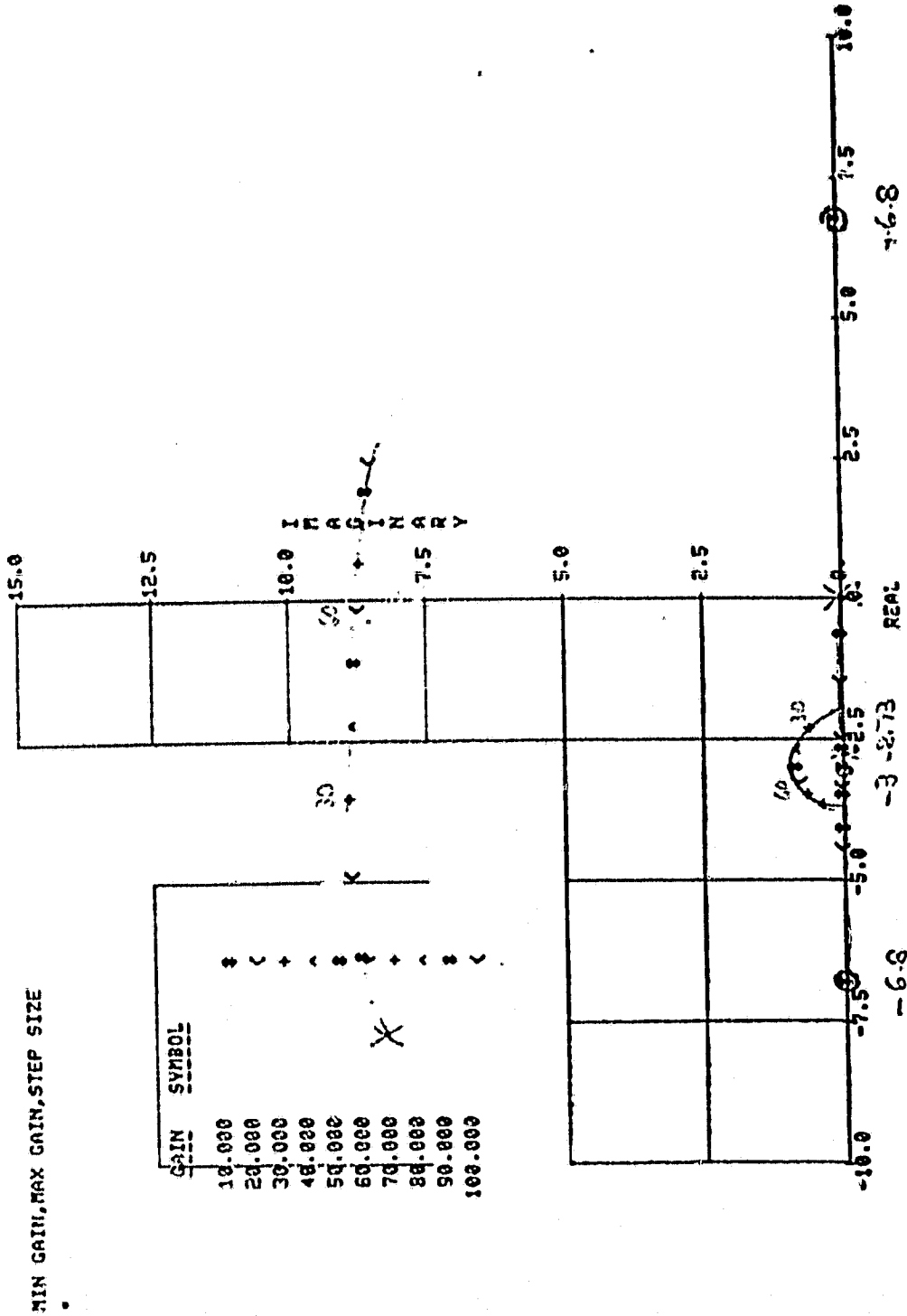
Closed coop control has been successfully achieved using the tachometer and the tip sensor only. The controller has been designed by root locus techniques; from the analysis done in II, it is easy to close the loop on the tachometer (rate): a simple gain is needed to stabilize the flexible poles. Figures 1 and 2 show the root locus then with the closed loop poles from the rate loop; the tip sensor loop is closed with a lead-lag network. Figures 3 and 4 show the root loci for 2 networks:

$$T = -k \frac{(s+3)}{(s+30)} y_T \ , \qquad T = -k \frac{(s+5)}{(s+30)} y_T$$

The control discussed above was implemented in analog electronics with very acceptable results. This control has limited bandwidth.

Research is now proceeding toward the long term objective described in Section I. It is believed that a control of high bandwidth can be achieved using the strain gages in addition to the other sensors. Also, more work needs to be done for the design of a command follower controller which can successfully slew the arm in a minimum amount of time.

A MINC II computer (PDP1103) has been acquired recently which will allow us to implement any sophisticated controller much more easily than with analog electronics.